Hyperactive ryanodine receptors in human heart failure and ischaemic cardiomyopathy reside outside of couplons

Eef Dries, Demetrio J. Santiago[†], Guillaume Gilbert, Ilse Lenaerts, Bert Vandenberk, Chandan K. Nagaraju, Daniel M. Johnson, Patricia Holemans, H. Llewelyn Roderick, Niall Macquaide[‡], Piet Claus, and Karin R. Sipido*

Department of Cardiovascular Sciences, KU Leuven, Campus Gasthuisberg, Herestraat 49 Box 704, B-3000 Leuven, Belgium

This article was handled by a consulting editor Ajay Shah.

Aims	In ventricular myocytes from humans and large mammals, the transverse and axial tubular system (TATS) network is less extensive than in rodents with consequently a greater proportion of ryanodine receptors (RyRs) not coupled to this membrane system. TATS remodelling in heart failure (HF) and after myocardial infarction (MI) increases the fraction of non-coupled RyRs. Here we investigate whether this remodelling alters the activity of coupled and non-coupled RyR sub-populations through changes in local signalling. We study myocytes from patients with end-stage HF, compared with non-failing (non-HF), and myocytes from pigs with MI and reduced left ventricular (LV) function, compared with sham intervention (SHAM).
Methods and results	Single LV myocytes for functional studies were isolated according to standard protocols. Immunofluorescent staining visualized organization of TATS and RyRs. Ca^{2+} was measured by confocal imaging (fluo-4 as indicator) and using whole-cell patch-clamp (37°C). Spontaneous Ca^{2+} release events, Ca^{2+} sparks, as a readout for RyR activity were recorded during a 15 s period following conditioning stimulation at 2 Hz. Sparks were assigned to cell regions categorized as coupled or non-coupled sites according to a previously developed method. Human HF myocytes had more non-coupled sites and these had more spontaneous activity than in non-HF. Hyperactivity of these non-coupled RyRs was reduced by Ca^{2+}/calmodulin-dependent kinase II (CaMKII) inhibition. Myocytes from MI pigs had similar changes compared with SHAM controls as seen in human HF myocytes. As well as by CaMKII inhibition, in MI, the increased activity of non-coupled sites was inhibited by mitochondrial reactive oxygen species (mito-ROS) scavenging. Under adrenergic stimulation, Ca^{2+} waves were more frequent and originated at non-coupled sites, generating larger Na^+/Ca^{2+} exchange currents in MI than in SHAM. Inhibition of CaMKII or mito-ROS scavenging reduced spontaneous Ca^{2+} waves, and improved excitation–contraction coupling.
Conclusions	In HF and after MI, RyR microdomain re-organization enhances spontaneous Ca^{2+} release at non-coupled sites in a manner dependent on CaMKII activation and mito-ROS production. This specific modulation generates a substrate for arrhythmia that appears to be responsive to selective pharmacologic modulation.
Keywords	Ryanodine receptor • Calcium • Calcium-calmodulin-dependent kinase II • Reactive oxygen species

---

* Corresponding author. Tel: +32 16 33 0815; fax: +32 16 34 5844, E-mail: karin.sipido@kuleuven.be

[†] Present address. Laboratory of Molecular Cardiology, Centro Nacional de Investigaciones Cardiovasculares Carlos III (CNIC), C. Melchor Fernández Almagro 3, 28029, Madrid, Spain

[‡] Present address. Institute of Cardiovascular and Medical Sciences, University of Glasgow, Neurosci and Biomedical Systems, Ibls, West Medical Building, Glasgow, UK

1. Introduction

Abnormal cellular Ca^{2+} handling and excitation-contraction coupling contribute to reduced contractile function and arrhythmogenesis in heart failure (HF).[1] Ca^{2+} uptake into the sarcoplasmic reticulum (SR) by SERCA, Ca^{2+} release through ryanodine receptors (RyRs), Ca^{2+} extrusion across the sarcolemma by the Na^+/Ca^{2+} exchanger (NCX), and Ca^{2+} influx via L-type Ca^{2+} channels (LTCCs) all contribute to this process. Novel Ca^{2+} pathways also emerge such as flux through TRP channels.[2] Functional changes in Ca^{2+} handling occur through alteration in protein expression or through post-translational modifications. Signalling pathways involved in remodelling of Ca^{2+} handling include those mediated by reactive oxygen species (ROS), Ca^{2+}/calmodulin-dependent kinase II (CaMKII), and nitric oxide (NO). Loss of SR Ca^{2+} through 'leaky' RyRs is attributed to post-translational modifications of RyRs that lead to alterations in RyR Ca^{2+} sensitivity and open probability (P_o). In animal models of disease, increased SR Ca^{2+} leak is observed after myocardial infarction (MI) compared with control[3] as well as in HF,[4] diabetes,[5] and atrial fibrillation (AF).[6] In human myocytes, greater Ca^{2+} leak was reported in HF[7] and AF[8,9] although one study found that spontaneous release events, Ca^{2+} sparks, were less frequent in HF.[10] Ca^{2+} loss through RyRs reduces contraction by decreasing the SR Ca^{2+} content, and can be a trigger to induce arrhythmogenic Ca^{2+} waves through activation of NCX.

Changes in the subcellular architecture of cardiac myocytes with disease further modulate Ca^{2+} handling. Reduced density and disorganization of the transverse and axial tubular system (TATS) is seen in post-MI remodelling.[11–13] These and other data suggest that TATS remodelling is a general feature in the progression to HF.[14] In contrast, RyR clusters appear to remain distributed at the Z lines throughout the cell, resulting in a large fraction of RyRs that are no longer in close proximity to the sarcolemmal (SL) membrane and TATS, i.e. outside couplons. Due to the increased distance to LTCCs, these non-coupled RyRs cannot be activated directly by Ca^{2+} entry via LTCC but are activated with a delay through Ca^{2+}-induced-Ca^{2+}-release propagating from coupled sites. This dys-synchrony reduces the rise time and amplitude of the global Ca^{2+} transient[12,15–17] and contributes to impaired contractile function.

The architecture of TATS results in different signalling microdomains around coupled and non-coupled RyRs. In healthy pig myocytes, coupled RyRs have a unique NOX2- and CaMKII-dependent regulation during increased heart rate and β-adrenergic stimulation.[18,19] However, the link between TATS remodelling in disease and the modulation of the larger population of non-coupled RyRs is not well studied.

To date, changes in RyR function in human HF have been exclusively studied at the myocyte level,[7,20] without information on subpopulations of RyRs, and mostly using HF myocytes only. Comparisons between non-HF and HF are scarce.[10] Recent work studied RyRs extracted from left ventricular (LV) tissues samples from HF and non-HF and reconstituted in bilayers.[21] In the pig with MI, we reported that TATS remodelling affected properties of the RyR subpopulations but did not investigate the signalling mechanisms involved.[22] In a dog model of HF, Belevych et al.[23] found that RyR subpopulations had different characteristics. However, little is known of the intrinsic properties, modulation, and arrhythmogenic contributions of coupled vs. non-coupled RyRs in post-MI remodelling or in human HF. Yet, selective targeting of modulators controlling RyR P_o has become of interest in the treatment of cardiac disease where impaired Ca^{2+} handling plays a role.[24–26]

Pilot data from our earlier work indicated that after MI, increased spontaneous RyR activity was exclusively a feature of non-coupled sites.

However, no mechanistic explanation could be offered at the time.[19] This study was designed: (i) to explore and validate the relevance of differences in coupled and non-coupled RyR properties in human HF; (ii) to study underlying mechanisms of the modulation of RyR subpopulations and the arrhythmogenic consequences in post-MI remodelling. Unlike in earlier work, here we induced MI in the anterior wall,[27] which has a larger impact on LV remodelling than MI in the posterior wall.[15,22]

2. Methods

Permission for the use of tissue from human hearts in the heart transplantation programme, explants, and non-used donor hearts, was obtained from the Ethical Committee of the University Hospital (UZ Leuven) with permit number S58824. The study conforms to the Helsinki declaration. Patients received usual care HF medication and data can be found in Supplementary material online, *Tables S1 and S2*.

Animals were housed and treated according to the Guide for the Care and Use of Laboratory Animals (National Institute of Health, USA), the European Directive 2010/63/EU and experimental protocols were approved by the in-house ethical committee (*Ethische Commissie Dierproeven*, KU Leuven), with permit numbers P10139, P14176, and P16110.

Cell isolation, confocal microscopy, and electrophysiological recordings were performed as previously described.[19] Single LV myocytes were enzymatically isolated from explanted human hearts[28] (failing, HF, and non-failing, non-HF) and from pigs with MI in the anteroseptal region, with reduced LV function and cellular remodelling[19,27] (see Supplementary material online, *Figures S1 and S2*). In human hearts, myocytes were obtained from the territory of the left anterior descendens coronary artery (LAD), cannulating a diagonal side-branch. If the LAD was not accessible, the left circumflex branch was used. In MI pigs, myocytes from the peri-infarct regions were prepared by cannulating a LAD side-branch and the same region was selected in SHAM animals. We used low (0.5 Hz) and high (2 Hz) frequency stimulation in the whole-cell voltage-clamp mode (-70 to +10 mV); the Ca^{2+} indicator fluo-4 was included in the pipette solution. Ca^{2+} sparks were recorded for 15 s after stimulation during confocal line-scan imaging. Cells were scanned along the longitudinal axis, orthogonal to the Z lines, avoiding scanning through nuclei. All experiments were performed at 37°C. Ca^{2+} sparks were assigned to coupled/non-coupled release sites based on an established algorithm.[19] A per-pixel spark frequency was calculated and normalized to give a measure in sparks/100 μm/s. Spark frequency was normalized to the length of the line in coupled/non-coupled sites. Ca^{2+} waves were induced at 2 Hz stimulation in the presence of isoproterenol (ISO; 10 nM). Ca^{2+} wave incidence was normalized to number of waves/100 μm/s and wave origins (pixel-based) were used to assign waves to coupled/non-coupled sites.

Immunofluorescent imaging was performed in fixed isolated cells or tissue sections. NCX was used as a surrogate marker to report on TATS membranes and distance masks were constructed as previously described.[19] From these masks, the fraction of coupled/non-coupled RyRs was calculated and co-localization of coupled/non-coupled RyRs with CaMKII was quantified according to the Manders' coefficient. To study TATS in relation to subcellular Ca^{2+} release, non-fixed myocytes were stained with wheat-germ-agglutinin-Alexa594 as described previously.[19]

Measurements of FAD/NAD(P)H for estimating redox potential were performed at 37°C under electrical field stimulation at various

frequencies by wide field fluorescence imaging using a Nikon TE2000 inverted microscope equipped with a 40 × 1.3 NA oil immersion objective and Hamamatsu Flash 4 CMOS camera. Endogenous fluorescent FAD and NAD(P)H signals were measured: NAD(P)H was excited at 360/10 nm and emission was collected at 480/40 nm (500 ms), FAD was excited at 485/20 nm and emission was collected at 535/30 nm (500 ms). Excitation and emission filters were selected using filter wheels (Sutter) and wavelengths discriminated using a triple band pass dichroic filter. Images were collected at a frequency of a ratio pair every 20 s.

2.1 Statistics

All data are presented as means ± SEM. For statistical analysis, we used a nested design taking into account n cells and N animals (freeware programme R, R Core Team (2013). R: A language and environment for statistical computing.), and Student's *t*-test or a two-way ANOVA with Bonferroni *post hoc* testing as applicable. The Fisher's exact test was used to compare incidence of Ca^{2+} waves between different groups. Data were considered significantly different when the probability value was < 0.05.

Detailed methods are provided in the Supplementary material online.
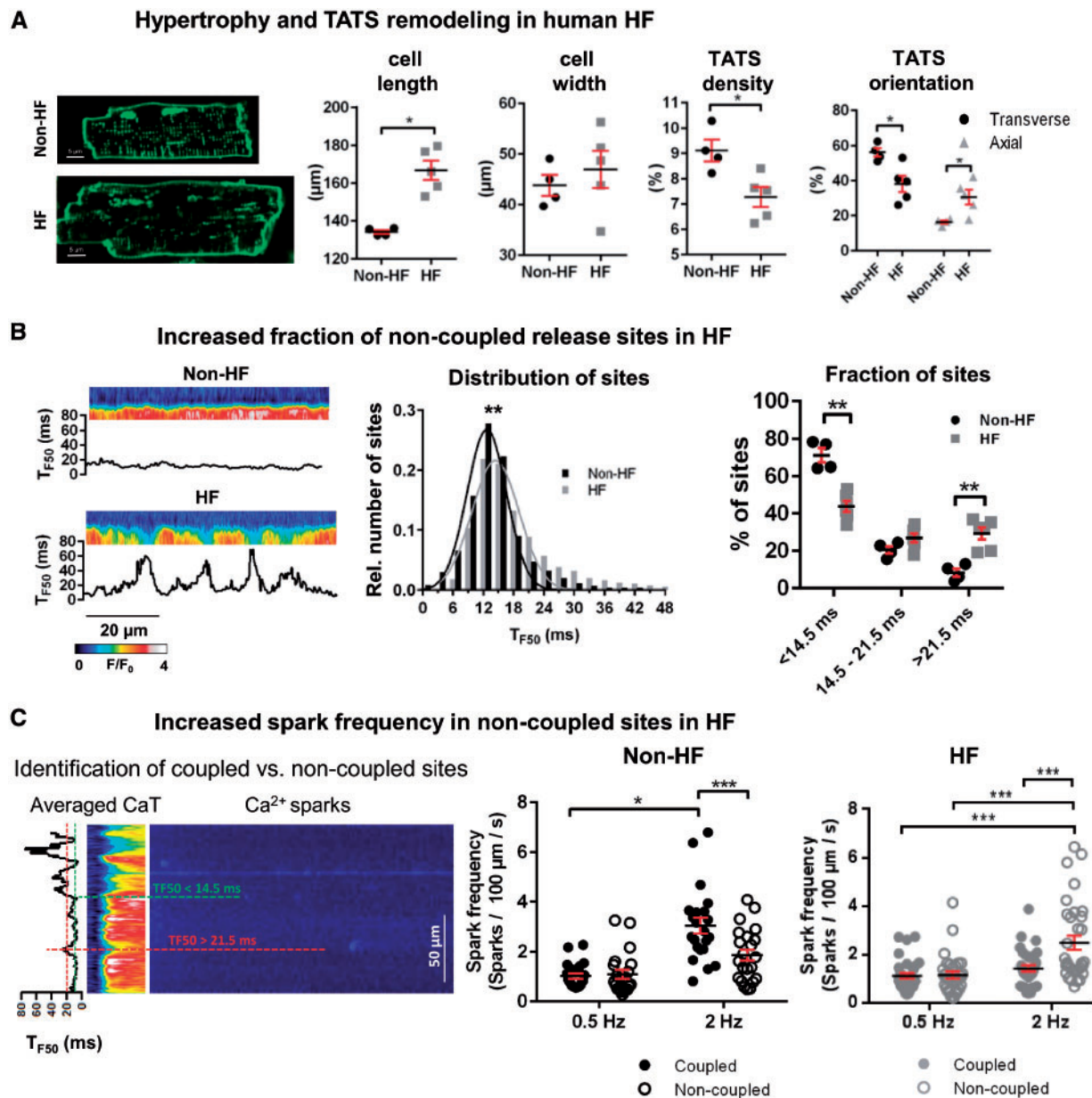
Figure 1 Myocyte hypertrophy and increased fraction of non-coupled release sites with an increased spark frequency in human HF. (*A*) Cell size and TATS characteristics in non-HF (n_{cells} = 27–31; N_{humans} = 4) and HF (n_{cells} = 83–91; n_{humans} = 5). Data are presented as mean value per subject. (*B*) *Left*: Examples of confocal line-scan recording of Ca^{2+} transients in non-HF and HF. Middle and right: Distribution and quantification of T_{F50} of the Ca^{2+} transient in coupled (<14.5 ms) and non-coupled (>21.5 ms) sites in non-HF (n_{cells} = 18; N_{humans} = 4) and HF (n_{cells} = 32; N_{humans} = 5). (*C*) *Left*: Example of a confocal line-scan recording using T_{F50} of the Ca^{2+} transient to assign sparks to different release sites. *Middle*: Spark frequency in coupled and non-coupled sites in non-HF (n_{cells} = 22; N_{humans} = 4) and *Right*: HF (n_{cells} = 32; N_{humans} = 6) (**P*-value < 0.05; ***P*-value < 0.01; ****P*-value < 0.001).

3. Results

3.1 Myocyte hypertrophy and increased fraction of non-coupled release sites in human HF

HF myocytes were longer than non-HF, without difference in cell width (*Figure 1A*). The density of TATS was significantly lower in HF myocytes and axial tubules were more abundant (*Figure 1A*).

To identify RyR subpopulations in human myocytes, we used a previously described algorithm,[19] establishing criteria as shown in the Supplementary material online, *Figure S3A*. These pre-established criteria allow studying of coupled and non-coupled release sites in a more rigorous way than used previously,[22,23] excluding intermediate release sites (between > 0.5 and < 2 μm) (see Supplementary material online, *Figure S4*). This approach still includes on average 80% of all release sites in all groups. As shown by its rightward shift, the distribution of the time to half-maximum of the Ca^{2+} transient (T_{F50}) for all release sites was significantly increased in HF myocytes (*Figure 1B*, middle). Quantification of early (coupled) and late (non-coupled) sites confirmed the decrease in the number of coupled sites and the increase of non-coupled sites in HF (*Figure 1B*, right). These data indicate that in human HF, hypertrophy is associated with an altered TAT network and an increased proportion of non-coupled release sites.

3.2 Increased activity of non-coupled release sites in HF, dependent on CaMKII

In non-HF myocytes, high-frequency stimulation caused a three-fold increase in spark frequency in coupled sites compared with that observed under low-frequency stimulation, whereas the spark frequency was only increased by 1.5-fold in non-coupled release sites (*Figure 1C*, middle). In HF myocytes, this frequency-dependent response was absent at coupled sites (*Figure 1C*, right), despite a substantial increase in SR Ca^{2+} load at 2 Hz in both HF and non-HF (*Figure 2B*); in HF SR Ca^{2+} content tended to be lower. In contrast, frequency of sparks at non-coupled sites in HF myocytes was significantly increased at 2 Hz (*Figure 1C*, right). The specific CaMKII inhibitor autocamtide-2-related-inhibitory-peptide (AIP) significantly reduced this hyperactivity in non-coupled regions without affecting spark frequency at coupled sites (*Figure 2A*).

3.3 Slower and smaller global Ca^{2+} transients in HF with beneficial effect of CaMKII inhibition

A reduced synchrony of Ca^{2+} release has previously been shown to lead to a slow rise of the Ca^{2+} transient in human HF myocytes.[17] Here we confirm that an increased fraction of non-coupled sites in HF myocytes in comparison to non-HF leads to a slower upstroke and reduced amplitude of the Ca^{2+} transient (*Figure 2B*). This dys-synchrony is further illustrated by the delay in the fraction of the line-scan that reached half-maximal Ca^{2+} release in HF myocytes compared with non-HF. Interestingly, inhibition of CaMKII that reduces diastolic release, removes the differences between HF and non-HF for amplitude and rate of upstroke (*Figure 2C*).

3.4 Specific modulation of coupled sites is lost after MI, whereas a *de novo* regulation appears at non-coupled release sites

Having established remodelling of TATS and spark properties in human HF, we used the post-MI pig model to gain further mechanistic understanding. The pig shares many features of cardiac physiology with humans, and ischaemic cardiomyopathy is the major cause of human HF. The relevance of the pig MI model is further underscored by earlier pilot data indicating that coupled and non-coupled release sites have properties similar to those seen here in human HF and CaMKII dependence was similar to human HF.[19]

In MI myocytes in the present study, likewise the CaMKII inhibitor AIP did not affect the spark frequency in coupled sites (*Figure 3A*), but reduced the spark frequency in non-coupled release sites (*Figure 3B*, see Supplementary material online, *Figure S5A* for baseline data). Global Ca^{2+} transients in MI myocytes were smaller with reduced rate of upstroke, as in HF, and consistent with the loss of TATS and reduced synchrony of Ca^{2+} release (see Supplementary material online, *Figure S5B*).

We further examined signalling and microdomains in the RyR subpopulations focussing on ROS as a candidate for post-MI signalling. NOX2 signalling is known to change in cardiac disease[29] and could be affected because of the TATS remodelling, while changes in metabolism and mitochondrial function[27] could affect mito-ROS production. In contrast to SHAM myocytes, inhibition of NOX2 with gp91 ds-tat peptide, did not affect the spark frequency in coupled sites after MI (*Figure 3A*). Since non-coupled sites lack TATS, NOX2-generated ROS at the TAT membrane is unlikely to affect non-coupled RyRs as confirmed by the lack of an effect of gp91 application (see Supplementary material online, *Figure S6*). Using the global ROS scavenger, NAC, we probed for ROS-mediated modulation from other sources. NAC significantly reduced the spark frequency in non-coupled sites (*Figure 3B*). None of these interventions affected the SR Ca^{2+} load (see Supplementary material online, *Figure S7B and C*).

## 3.5 CaMKII and NOX2 localization is intact after MI

The lack of frequency-response in coupled release sites after MI could be attributed to the specific loss of CaMKII and/or NOX2 in coupled regions. In both SHAM and MI myocytes, there was however a similar degree of co-localization between CaMKII and coupled or non-coupled RyRs (*Figure 4Aa*). No change in CaMKII expression in SHAM and MI tissue was detected (see Supplementary material online, *Figure S8*). The localization of NOX2 at the TATS was intact after MI (*Figure 4Ab*, see Supplementary material online, *Figure S9A and B*).

3.6 Reduced [Ca^{2+}] and ROS scavenging in the dyadic cleft after MI

A potential mechanism for the lack of CaMKII activation in coupled regions after MI remodelling is the loss of high Ca^{2+} microdomains in the dyadic cleft. We analysed local [Ca^{2+}] by measuring I_{CaL} inactivation and local Ca^{2+} transient kinetics. The early inactivation of I_{CaL} was decreased (larger Tau_{fast}), indicating reduced [Ca^{2+}] near LTCC (*Figure 4B*). In addition, the amplitude and rate of upstroke of Ca^{2+} transients in regions of coupled sites were reduced (see Supplementary material online, *Figure S5C*).

We tested the hypothesis that changes in NOS1 could reduce ROS in the dyadic cleft, as e.g. produced by local NOX2 (*Figure 4C*). Recently, local ROS scavenging mechanism at the SR have been described, whereby NOS1-derived NO can scavenge xanthine oxidase (XO)-produced ROS.[30] During disease, NOS1 has been shown to translocate from the SR to the TATS.[31] Translocated NOS1-derived NO at the TATS could thus mask a local ROS microdomain by scavenging ROS produced by NOX2 in MI myocytes. Inhibition of NOS1 with L-NAME, and with the more specific L-VNIO produced a significant increase in the spark frequency in coupled sites in MI myocytes to a similar level as in control.
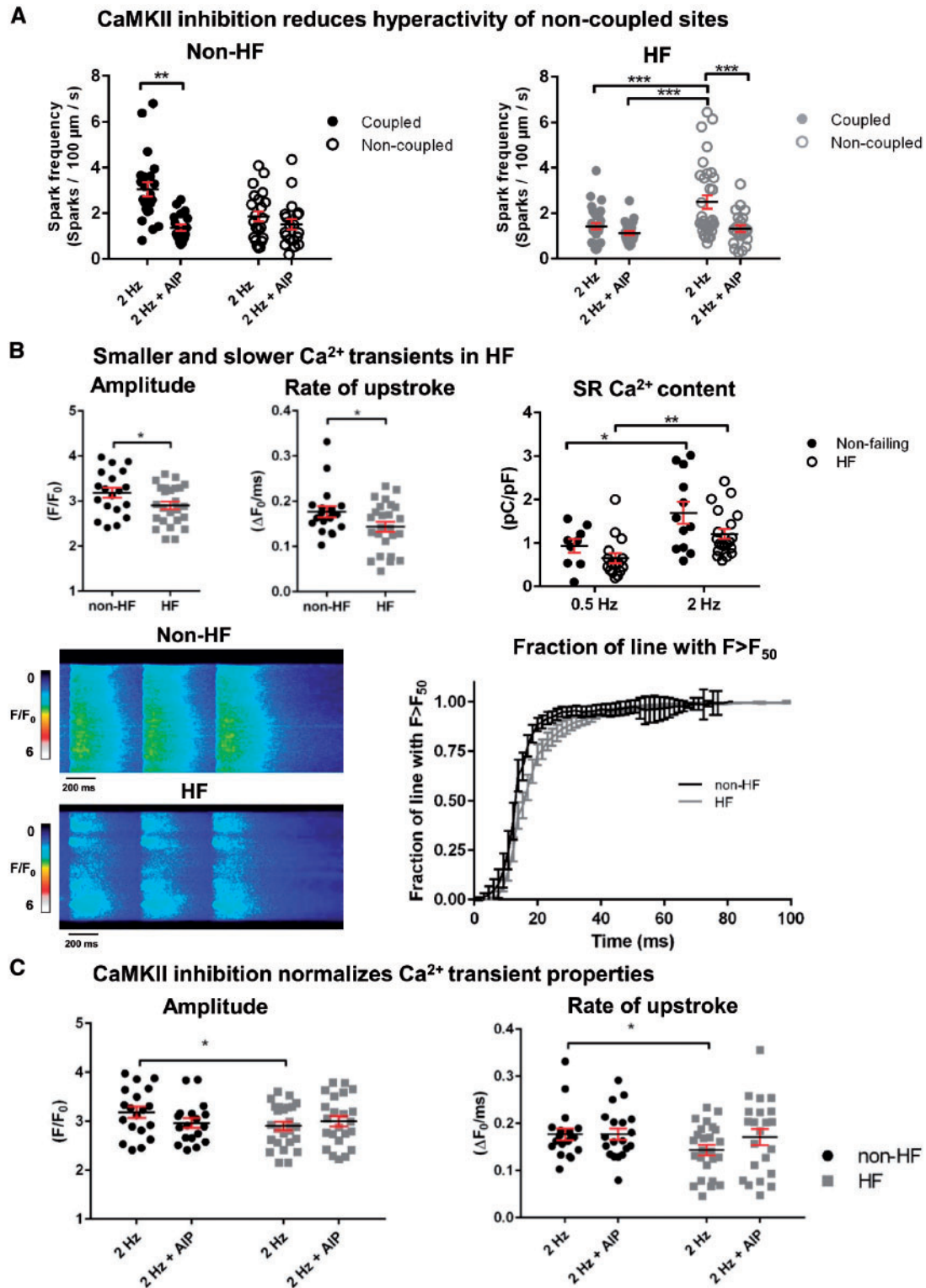
Figure 2 CaMKII inhibition normalized both RyR activity and Ca^{2+} transients in human HF myocytes. (*A*) The effect of AIP in coupled and non-coupled sites in non-HF (n_{cells} = 19; N_{humans} = 4) and HF (n_{cells} = 23; N_{humans} = 6). (*B*) Ca^{2+} transient amplitude in non-HF (n_{cells} = 19; N_{human} = 4) and HF (n_{cells} = 25; N_{human} = 6) at 2 Hz stimulation with examples of line-scan and reduced synchrony. The fraction of the line-scan with at least half-maximal Ca^{2+} release as a function of time. SR Ca^{2+} content in non-HF and HF at 0.5 Hz (n_{cells} = 8; N_{humans} = 4 in non-HF; n_{cells} = 16; N_{humans} = 6 in HF) and 2 Hz (n_{cells} = 11; N_{humans} = 4 in non-HF; n_{cells} = 20; N_{humans} = 6 in HF). (*C*) Ca^{2+} transient amplitude in non-HF (n_{cells} = 19; N_{human} = 4) and HF (n_{cells} = 25; N_{human} = 6) at 2 Hz and the effect with AIP (non-HF: n_{cells} = 19; N_{human} = 4 and HF: n_{cells} = 23; N_{human} = 6) (**P*-value < 0.05; ***P*-value < 0.01; ****P*-value < 0.001).
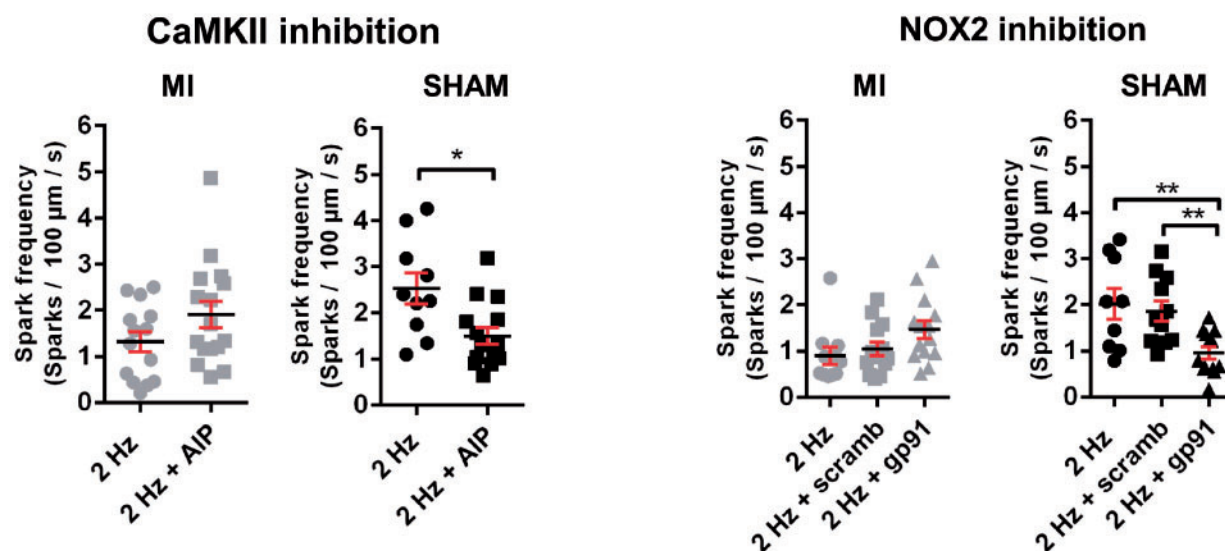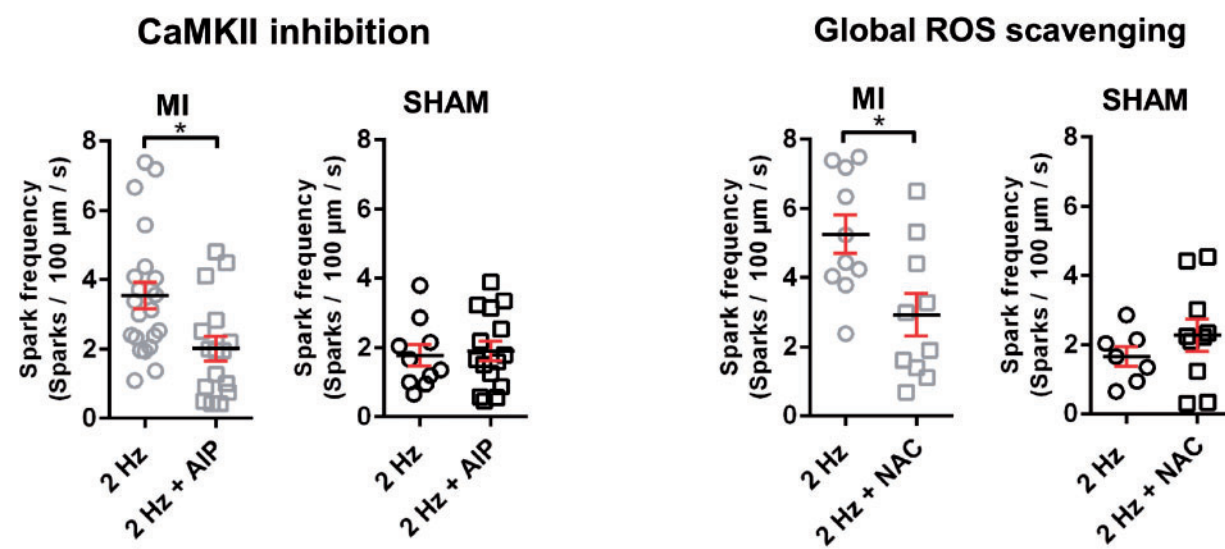
Figure 3 CaMKII-dependent and ROS-dependent signalling examined at coupled vs. non-coupled sites after MI in pig ventricular myocytes. (A) *Left:* The effect of AIP in coupled sites in MI (n_{cells} = 16; N_{pigs} = 7) and SHAM (n_{cells} = 15; N_{pigs} = 4). *Right:* The effect of gp91 ds-tat peptide in coupled sites in MI (n_{cells} = 14; N_{pigs} = 4) and SHAM (n_{cells} = 13; N_{pigs} = 4). (B) *Left:* The effect of AIP in non-coupled sites in MI (n_{cells} = 16; N_{pigs} = 7) and SHAM (n_{cells} = 15; N_{pigs} = 4). *Right:* The effect of NAC in non-coupled sites in MI (n_{cells} = 10; N_{pigs} = 5) and SHAM (n_{cells} = 10; N_{pigs} = 3) (*P-value < 0.05; **P-value < 0.01).

NOS inhibition did not affect the frequency-response in coupled sites in SHAM myocytes (*Figure 4C*).

3.7 ROS from mitochondria modulate non-coupled RyRs after MI

The data in *Figure 3B* imply that there must be an alternative ROS source to NOX2 affecting the non-coupled sites in MI. We hypothesised that the mitochondria were responsible. Scavenging mitochondrial ROS (mito-ROS) using mitoTEMPO significantly reduced spark frequency at

non-coupled regions in MI, without affecting coupled sites (*Figure 5A*); there was no effect in SHAM. SR Ca^{2+} content was unchanged by this manoeuver in SHAM or MI (see Supplementary material online, *Figure S7B and C*). Inhibition of XO with oxypurinol had no effect on sparks in either SHAM or MI myocytes (see Supplementary material online, *Figure S10*) indicating that this enzyme did not contribute to ROS generation. These observations raised the question whether pacing at 2 Hz selectively induced mito-ROS in MI but not in SHAM. To test this possibility, we studied cellular redox potential through measuring the FAD/NAD(P)H ratio. During stimulation at 2 Hz, the NAD(P)H signal
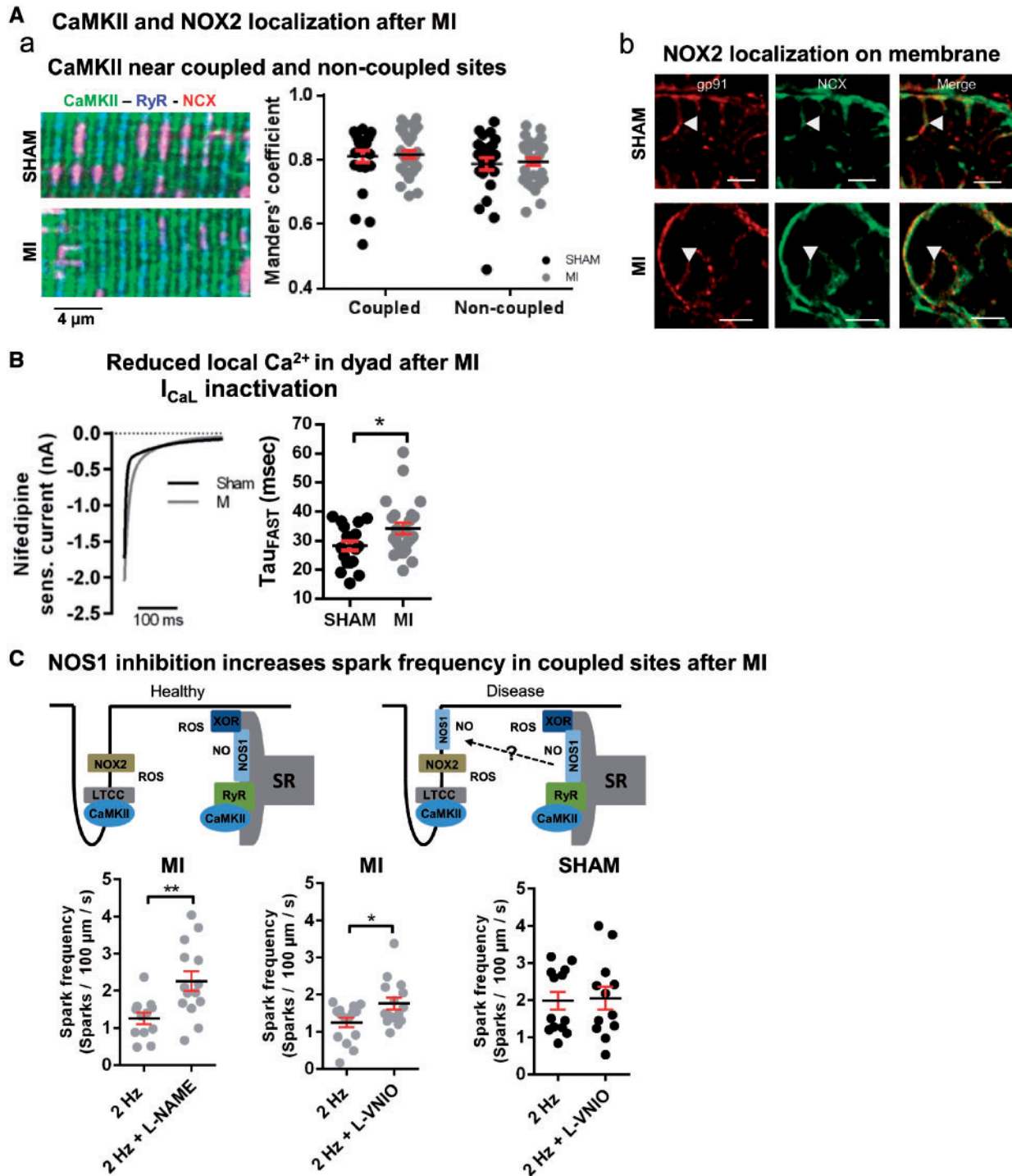
Figure 4 Ca^{2+} and ROS in the dyadic cleft after MI in pig myocytes. (*A*) *a*. Example of a confocal image of a pig ventricular myocyte stained for RyR (blue), CaMKII (green), and NCX (red). The co-localization of CaMKII in coupled and non-coupled RyRs is shown using the Manders' coefficient in SHAM (n_{cells} = 26; N_{pigs} = 6) and MI (n_{cells} = 32; N_{pigs} = 7). *b*. Example of tissue samples in SHAM and MI stained for gp91 (red), NCX (green) and overlay (yellow). Scale bar equals 5 μm. (*B*) Example and mean values of I_{CaL} inactivation in SHAM (n_{cells} = 19; N_{pigs} = 3) and MI (n_{cells} = 24; N_{pigs} = 5). (*C*) The effect of L-NAME (n_{cells} = 14; N_{pigs} = 4) and L-VNIO (MI: n_{cells} = 15; N_{pigs} = 4; SHAM: n_{cells} = 12; N_{pigs} = 3) in coupled sites in MI and SHAM (*P-value < 0.05; **P-value < 0.01; ***P-value < 0.001).
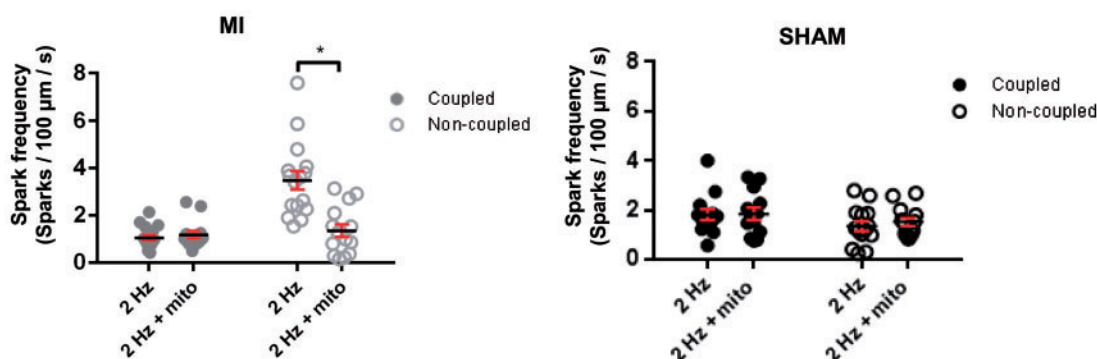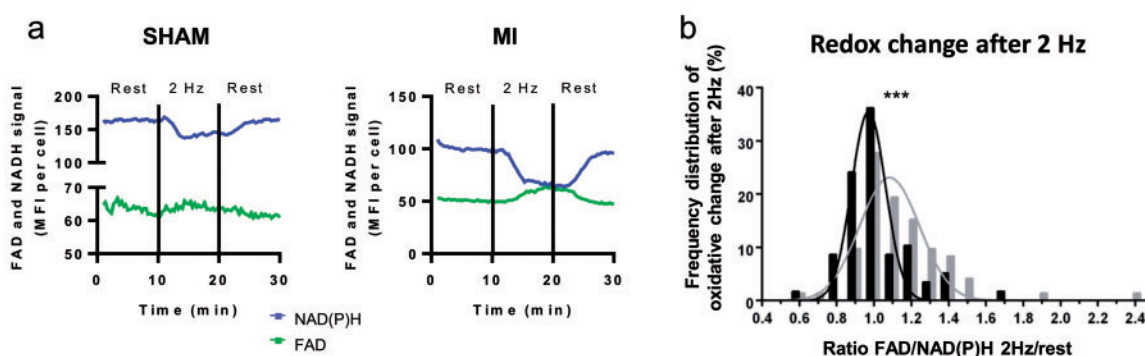
Figure 5 Mito-ROS microdomain affects non-coupled sites after MI in pig myocytes. (*A*) The effect of mitoTEMPO on spark frequency in coupled and non-coupled sites in MI (n_{cells} = 14; N_{pigs} = 4) and SHAM (n_{cells} = 13; N_{pigs} = 5). (*B*) *a*. Example traces of NAD(P)H and FAD signals, measured over time as the mean fluorescence intensity, in SHAM and MI at 2 Hz. *b*. For each cell, the FAD/NAD(P)H ratio measured after pacing at 2 Hz was normalized to the rest value. The graph represents the frequency distribution with the fitted Gaussian curves in SHAM and MI (*P-value < 0.05; ***P-value < 0.001).

decreased while the FAD signal increased. Comparison of the ratio of these changes between SHAM and MI revealed a greater increase in FAD/NAD(P)H in MI myocytes (*Figure 5Bb*).

3.8 After MI, Ca^{2+} waves are more frequent and originate in non-coupled release sites

Increased RyR activity/sensitivity may result in spontaneous Ca^{2+} waves that promote arrhythmias. We investigated the susceptibility for Ca^{2+} waves in MI during β-adrenergic stimulation at 2 Hz, mimicking the *in vivo* adrenergic effects.

MI myocytes exhibited more Ca^{2+} waves than SHAM, and these Ca^{2+} waves generated significantly larger NCX currents (I_{NCX}) (*Figure 6B*). This was reflected by an increased number and amplitude of delayed-afterdepolarizations (DADs) as well as an increase in number of spontaneous action potentials (APs) (*Figure 6C*). We related the source of Ca^{2+} waves to either coupled and non-coupled sites based on the T_{F50} of the Ca^{2+} transient. A distribution plot shows that after MI, Ca^{2+} waves originated more frequently from non-coupled sites (*Figure 6D*).

To induce triggered activity, and ultimately arrhythmias, membrane depolarization by the inward I_{NCX} generated by the Ca^{2+} waves must reach the threshold for AP generation. Larger I_{NCX} is generated when multiple Ca^{2+} waves collide. In MI, more cells exhibited colliding Ca^{2+} waves compared with SHAM (*Figure 6Ea*). These colliding waves had a larger amplitude

and I_{NCX} compared with single Ca^{2+} waves in MI myocytes (see Supplementary material online, *Figure S11*). Colliding waves originating from non-coupled sites had the highest peak and integrated I_{NCX} (*Figure 6Eb*).

3.9 Inhibition of CaMKII and mito-ROS reduces Ca^{2+} waves from non-coupled sites in MI

In MI myocytes, mitoTEMPO and AIP reduced the increased wave frequency originating from non-coupled sites without significantly affecting those arising from coupled regions (*Figure 7A*). Direct inhibition of RyR opening with flecainide or S107 reduced Ca^{2+} waves in both MI and SHAM.

We assessed the impact of these interventions on excitation-contraction coupling and the Ca^{2+} transient. Flecainide, CaMKII and mitoTEMPO did not affect the Ca^{2+} transient amplitude, whereas S107 significantly reduced the amplitude in both SHAM and MI myocytes (*Figure 7B*).

4. Discussion

TATS remodelling in ventricular myocytes after MI and in HF, leads to an increase in non-coupled release sites. Unlike in the healthy heart, these
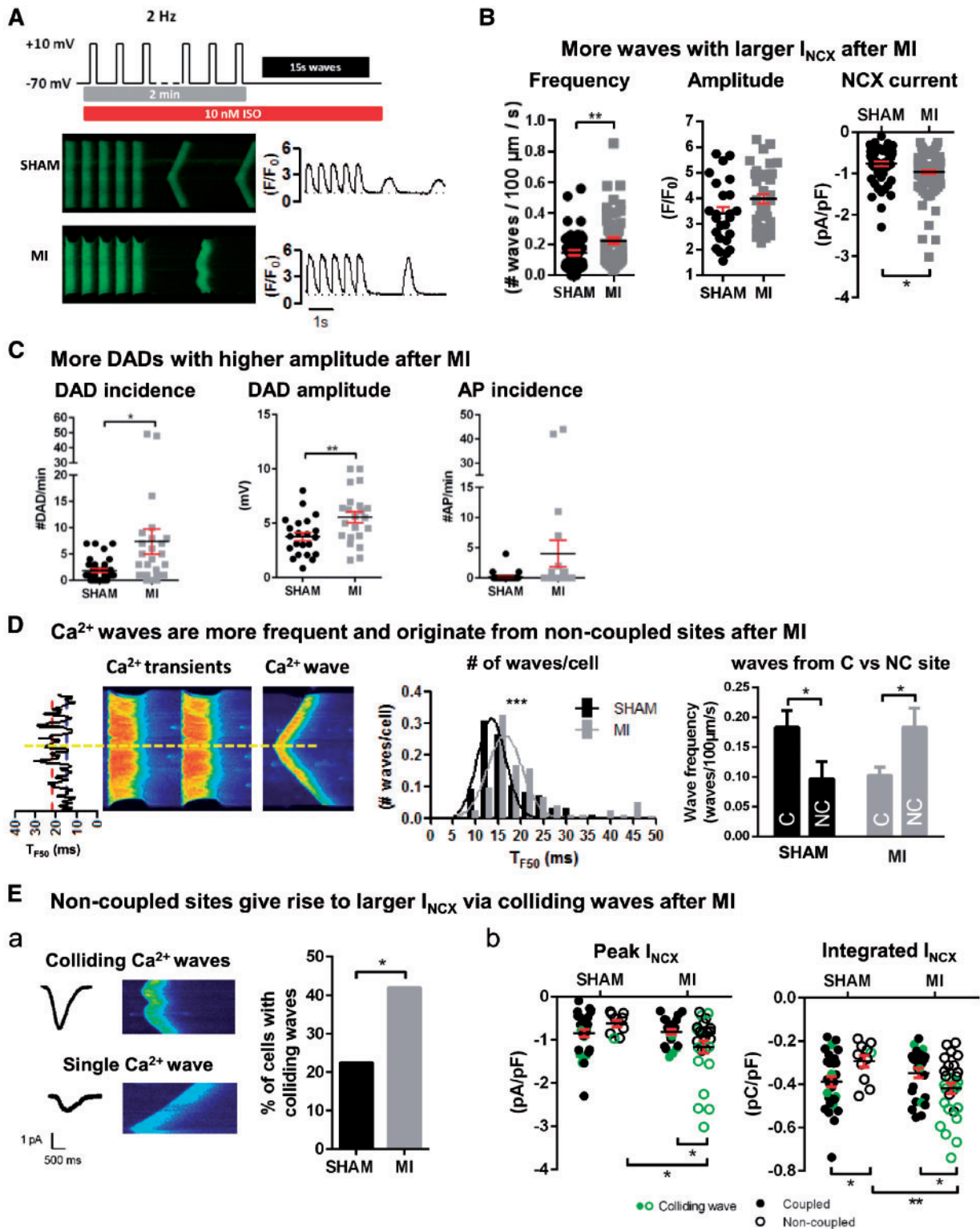
Figure 6 Ca^{2+} wave frequency increases and Ca^{2+} wave origin shifts towards non-coupled release sites after MI in pig myocytes. (*A*). Examples of Ca^{2+} waves in SHAM and MI are shown. (*B*) Wave frequency (SHAM: n_{cells} = 59; N_{pigs} = 13, MI: n_{cells} = 62; N_{pigs} = 16), wave-induced Ca^{2+} transient amplitude (SHAM: n_{waves} = 30 in n_{cells} = 25 in N_{pigs} = 9; MI: n_{waves} = 49 in n_{cells} = 38 in N_{pigs} = 11) and wave-induced I_{NCX} (SHAM: n_{waves} = 59 in n_{cells} = 32 in N_{pigs} = 9; MI: n_{waves} = 91 in n_{cells} = 38 in N_{pigs} = 11) for SHAM and MI. (*C*) DAD incidence, DAD amplitude and spontaneous APs in SHAM (n_{cells} = 28; N_{pigs} = 6) and MI (n_{cells} = 34; N_{pigs} = 7). (*D*) *Left*: Waves are assigned to coupled or non-coupled release sites by using the wave origin (pixel-based) and T_{F50} of the Ca^{2+} transient. *Middle*: The distribution of wave origins and *Right*: wave frequency in SHAM (n_{cells} = 39; N_{pigs} = 9) and MI (n_{cells} = 62; N_{pigs} = 16). (*E*) *a*. Example and quantification of colliding and single waves in SHAM and MI. *b*. Ca^{2+} wave peak I_{NCX} and integrated I_{NCX} in coupled and non-coupled sites in SHAM and MI. Colliding waves are indicated in green. Only colliding waves are included when originating from only coupled or non-coupled sites. (n_{waves} = 11–28, n_{cells} = 32–38, N_{pigs} = 9–11) (*P*-value < 0.05; **P*-value < 0.01; ***P*-value < 0.001).
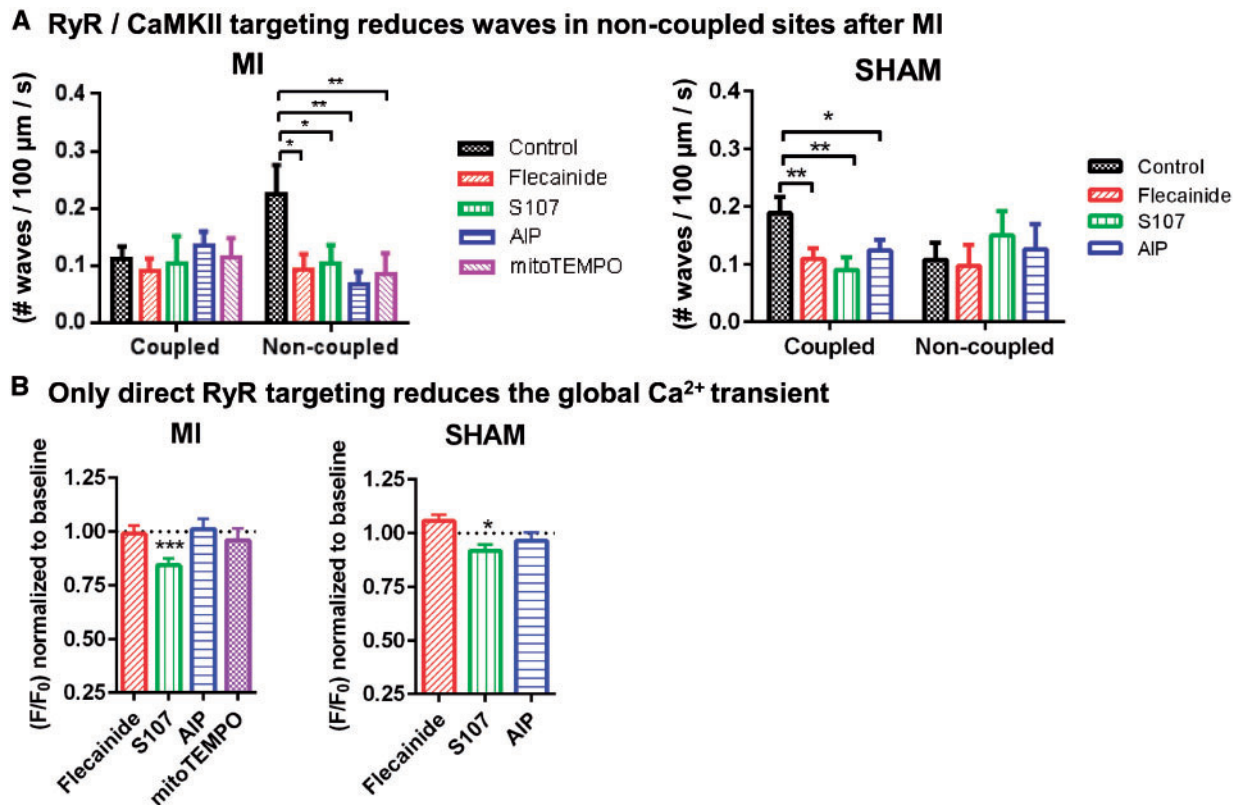
Figure 7 Non-coupled release sites are more sensitive to RyR blockers and inhibition of RyR modulators after MI in pig myocytes. (*A*) Effects of flecainide (SHAM: n_{cells} = 27; N_{pigs} = 5; MI: n_{cells} = 26; N_{pigs} = 6), S107 (SHAM: n_{cells} = 19; N_{pigs} = 3; MI: n_{cells} = 27; N_{pigs} = 4), AIP (SHAM: n_{cells} = 22; N_{pigs} = 3; MI: n_{cells} = 25; N_{pigs} = 9) and mitoTEMPO (MI: n_{cells} = 23; N_{pigs} = 5) on (*A*) wave frequency and (*B*) global Ca^{2+} transient in SHAM and MI (*P-value < 0.05; **P-value < 0.01).

sites, outside of couplons, exhibit increased spontaneous activity during diastole at higher heart rates. This arises through distinct alterations in Ca^{2+} and ROS microdomains around the different RyR populations. After MI, non-coupled release sites are at the origin of Ca^{2+} waves. These Ca^{2+} waves generate larger depolarizing currents by simultaneously activating multiple Ca^{2+} release sites, thereby highlighting the arrhythmogenic potential of these sites.

4.1 TATS remodelling in human HF impacts on RyR activity and global Ca^{2+} transient properties

We observed a significant reduction in TATS density, predominantly of the T-tubules (TTs) in HF, extending earlier studies in human tissue. Early electron microscopy studies described dilated TTs.[32] Other features previously described include an irregular distribution,[11,17] an increase in TT diameter[11] and a reduction in TT density.[33–35]

TATS remodelling results in an increased fraction of non-coupled RyR cluster sites, in line with data from a canine model of HF[36] and human HF myocytes.[35] This remodelling is associated with loss of synchrony and reduced amplitude of the Ca^{2+} transient through delayed opening of the non-coupled RyRs. Similar findings were reported in animal models[12,13,15] but data from human HF are scarce or did not include information from non-HF myocytes.[17,35]

This study also adds new information regarding the intrinsic properties of RyRs clusters at coupled and non-coupled sites. Indeed, previous studies have only reported on overall RyR activity recorded as sparks in diastole and in lipid bilayer experiments, without distinguishing subpopulations.[7,21,37] They mostly report an increase in total spark frequency, although Lindner et al.[10] reported a decrease in HF. An important difference between the aforementioned study and ours is that we studied cells under voltage-clamp. The voltage-clamp mode with controlled membrane potential and equal duration of membrane depolarization achieves a more equal SR load and Ca^{2+} fluxes allowing better dissection of RyR properties with less influence of confounding factors (including disease associated remodelling of the AP and resting membrane potential). Our finding that the spark activity in non-coupled sites is sensitive to CaMKII inhibition is in line with previous reports on RyR properties in HF, although a comparison to non-HF was not included in those studies.[7,37] Recently, lipid bilayer experiments on RyR activity support these findings, with a major role for RyR phosphorylation and thiol oxidation in HF conditions.[21] In line with the study from Fischer et al.,[7] no differences in response to CaMKII inhibition were found between myocytes from ischaemic and dilated cardiomyopathy (see Supplementary material online, Figure S12). The data complement earlier work on the global assessment of Ca^{2+} transients in HF vs. non-HF human myocytes.[38] Our data further show that in HF, CaMKII inhibition can reduce diastolic events with favourable effects on the global Ca^{2+} transient.

4.2 Loss of dyadic cleft CaMKII signalling after MI

Despite its presence at both coupled and non-coupled RyR clusters, we did not detect CaMKII activation in the dyadic cleft near coupled sites in MI, an effect possibly due to reduced $[Ca^{2+}]$ in this microdomain.[39] This could be a primary event after MI with several potential causes. The SR Ca^{2+} content is not reduced, excluding this possibility. Reduced coupling gain between LTCC and RyR is another possibility, as in the rabbit with HF.[16,40] Litwin *et al.*[16] proposed a different molecular configuration of LTCC as the underlying mechanism whereas Bryant *et al.* reported a re-distribution of I_{CaL} away from the TT.[40,41] Another possibility is the structure of the RyR cluster. Cluster size and organization affect P_o[42,43] and may change in disease as recently reported for AF.[44]

Furthermore, Erickson *et al.*[45] recently reported that exposure to NO prior to Ca^{2+}/CaM binding to CaMKII strongly suppresses CaMKII activity. This could explain the loss of CaMKII activation in coupled regions after MI, in line with the increased spark frequency with NOS in-hibition. NO production may mask the ROS microdomain through translocation of NOS1 from the SR to the TATS. This may be through ROS in the dyadic cleft or ROS from mitochondrial sources.

Another possible mechanism may be through dysregulation of local-ized antioxidant mechanisms. Glyceraldehyde 3-phosphate dehydroge-nase, located at the TATS,[46] potentially regulates the redox state at SR–SL junctions by the production of NADH. In support of this notion, ischaemic and dilated cardiomyopathies are known to cause a shift in metabolic substrate utilization from free fatty acids to glucose,[27,47] thereby increasing the rate of glycolysis and associated NADH produc-tion, resulting in ROS scavenging at the dyadic cleft.

4.3 Non-coupled release sites have increased spontaneous activity

Our data show a *de novo* form of modulation of non-coupled sites, de-pendent on CaMKII activation and mito-ROS. Increased CaMKII activity in the regulation of RyRs has been associated with several cardiac dis-eases[7,37,48,49] but its selective activation at non-coupled regions was so far not reported. The low rate of upstroke of triggered Ca^{2+} release in non-coupled regions makes it unlikely that CaMKII is activated by Ca^{2+} in non-coupled regions. Instead, our data suggest a more prominent role for mito-ROS, rather than Ca^{2+}, in the activation of CaMKII, as recently shown in diabetic mouse heart.[50] Moreover, increased levels of mito-ROS manifest in patients[51] and animals with advanced HF.[52–54]

The increased activity of RyRs at non-coupled sites in MI occurs without apparent change in SR Ca^{2+} content. We could not yet study the full rela-tionship between SR leak and content.[55] It is conceivable that our experi-ments occur at the exponential part of this relationship together with a shift in the curve due to RyR post-translational modifications. Therefore, one can have increased leak with small or no changes in SR Ca^{2+} content.

4.4 Non-coupled sites are hotspots for arrhythmogenic Ca^{2+} waves

The increased wave frequency that we observe make non-coupled RyR clusters a potential source of deleterious Ca^{2+} handling in MI. In contrast, Belevych *et al.*[23] recently proposed that potential arrhythmo-genic Ca^{2+} waves arise from coupled sites in myocytes from the dog with pacing-induced HF. This opposing finding may reflect species differences and different types of remodelling, as there was no loss of TT in this HF model. Also, differences in experimental conditions may help to explain the different findings between the two studies. Belevych

et al.[23] recorded at room temperature and 0.5 Hz pacing, in contrast to $37°C$ and 2 Hz pacing frequency in this study. Of note, at 0.5 Hz condi-tioning, we did not see the distinguishing activity between coupled and non-coupled RyRs.

Inhibition of diastolic RyR Ca^{2+} leak could be a therapeutic strategy with direct RyR block or modulation.[24–26] In this study, Ca^{2+} waves were reduced by both RyR blockade and inhibition of RyR modulation. The S107 and flecainide-dependent reduction in Ca^{2+} wave frequency is in line with data previously reported under various conditions,[24,26] although how flecainide reduces Ca-wave dependent arrhythmias is debated.[56]

The role of CaMKII in arrhythmias has been previously investigated,[57] including ROS-induced CaMKII activation.[58,59] Here we show that CaMKII inhibition in MI selectively reduced waves originating from non-coupled RyRs without adverse effects on coupled RyRs and excitation-contraction coupling. CaMKII inhibition or mito-ROS scavenging would thus be better strategies than direct RyR inhibition, which is less discriminating.

Last, the impact of waves on depolarizing currents was larger in MI. This may at first glance be counterintuitive as non-coupled sites are more dis-tant from the membrane. However, this distance may also cause a tempo-rary increased re-circulation of Ca^{2+} in the stores with eventually larger cell-wide Ca^{2+} release, colliding waves, larger I_{NCX}, and ultimately, trig-gered activity. In a pilot study, *in vivo* monophasic AP from the peri-infarct region during 2 Hz pacing and isoproterenol support the occurrence of high amplitude DADs (see Supplementary material online, *Figure S13*), whereas only low amplitude DADs were observed in SHAM animals. In three out of five MI pigs, this pro-arrhythmic pacing protocol triggered premature ventricular complexes *in vivo*. This was rarely observed in SHAM animals.

4.5 Limitations and future directions

Human samples are limited in nature and quantity and not available for all experiments. Nevertheless, our key observations in pig suggest com-parable mechanisms after disease remodelling in human HF myocytes.

In this study, only indirect and global ROS measurements were used although development of local ROS measurements could provide further insights. For local $[Ca^{2+}]$, targeted probes are available but cell culture[60–62] complicates the application as culture affects TT ultrastructure.

Our biochemical characterization of RyR and CaMKII modifications remains limited. No differences were found for the direct oxidation of RyR between SHAM and MI tissues (see Supplementary material online, *Figure S14A*). Immunostainings for both phosphorylation and oxidation of CaMKII showed a significant increase in MI myocytes (see Supplementary material online, *Figure S14B and C*). These approaches are however not sufficient to detect dynamic changes during live cell experiments at the subcellular level. In the current experiments, we have relied on pharmacological tools and despite the use of different agents and controls, there is always the potential for non-selective or indirect effects. This limitation was preferred over gene manipulation that requires cell culture, introducing other potential confounders.

In this work, a fraction of nearly 20% of non-coupled RyRs was ob-served in SHAM pig myocytes using functional and immunostaining methods (see Supplementary material online, *Figure S1*). This is high compared with studies in human tissues, including present data, and dog myocytes.[35,63] Species-specific and methodological differences might ac-count for some of this apparent disparity. Here and in our previous work,[19] we predominantly rely on the relationship between SR Ca^{2+} re-lease and TATS distance to identify RyR subgroups. If not all RyRs are ac-tive this may introduce discrepancies.

5. Conclusion

In HF and after MI, RyR microdomain organization enhances spontaneous Ca^{2+} release and sparks from non-coupled sites, in a manner that is dependent on CaMKII activation and mito-ROS production. This specific modulation may generate a substrate for arrhythmia that appears to be responsive to selective pharmacologic modulation.

Supplementary material

Supplementary material is available at *Cardiovascular Research* online.

References

1. Luo M, Anderson ME. Mechanisms of altered Ca^{2+} handling in heart failure. *Circ Res* 2013;**113**:690–708.
2. Lorin C, Vögeli I, Niggli E. Dystrophic cardiomyopathy: role of TRPV2 channels in stretch-induced cell damage. *Cardiovasc Res* 2015;**106**:153–162.
3. Fauconnier J, Meli AC, Thireau J, Roberge S, Shan J, Sassi Y, Reiken SR, Rauzier J-M, Marchand A, Chauvier D, Cassan C, Crozier C, Bideaux P, Lompré A-M, Jacotot E, Marks AR, Lacampagne A. Ryanodine receptor leak mediated by caspase-8 activation leads to left ventricular injury after myocardial ischemia-reperfusion. *Proc Natl Acad Sci U S A* 2011;**108**:13258–13263.
4. Terentyev D, Györke I, Belevych AE, Terentyeva R, Sridhar A, Nishijima Y, Blanco ECD, Khanna S, Sen CK, Cardounel AJ, Carnes CA, Györke S. Redox modification of ryanodine receptors contributes to sarcoplasmic reticulum Ca2+ leak in chronic heart failure. *Circ Res* 2008;**103**:1466–1472.
5. Yaras N, Ugur M, Ozdemir S, Gurdal H, Purali N, Lacampagne A, Vassort G, Turan B. Effects of diabetes on ryanodine receptor Ca release channel (RyR2) and Ca2+ homeostasis in rat heart. *Diabetes* 2005;**54**:3082–3088.
6. Li N, Chiang DY, Wang S, Wang Q, Sun L, Voigt N, Respress JL, Ather S, Skapura DG, Jordan VK, Horrigan FT, Schmitz W, Müller FU, Valderrabano M, Nattel S, Dobrev D, Wehrens XHT. Ryanodine receptor-mediated calcium leak drives progressive development of an atrial fibrillation substrate in a transgenic mouse model. *Circulation* 2014;**129**:1276–1285.
7. Fischer TH, Eiringhaus J, Dybkova N, Förster A, Herting J, Kleinwächter A, Ljubojevic S, Schmitto JD, Streckfuß-Bömeke K, Renner A, Gummert J, Hasenfuss G, Maier LS, Sossalla S. Ca(2+)/calmodulin-dependent protein kinase II equally induces sarcoplasmic reticulum Ca(2+) leak in human ischaemic and dilated cardiomyopathy. *Eur J Heart Fail* 2014;**16**:1292–1300.
8. Hove-Madsen L, Llach A, Bayes-Genís A, Roura S, Rodriguez Font E, Arís A, Cinca J. Atrial fibrillation is associated with increased spontaneous calcium release from the sarcoplasmic reticulum in human atrial myocytes. *Circulation* 2004;**110**:1358–1363.
9. Neef S, Dybkova N, Sossalla S, Ort KR, Fluschnik N, Neumann K, Seipelt R, Schöndube FA, Hasenfuss G, Maier LS. CaMKII-dependent diastolic SR Ca2+ leak and elevated diastolic Ca2+ levels in right atrial myocardium of patients with atrial fibrillation. *Circ Res* 2010;**106**:1134–1144.
10. Lindner M, Brandt MC, Sauer H, Hescheler J, Böhle T, Beuckelmann DJ. Calcium sparks in human ventricular cardiomyocytes from patients with terminal heart failure. *Cell Calcium* 2002;**31**:175–182.
11. Cannell MB, Crossman DJ, Soeller C. Effect of changes in action potential spike configuration, junctional sarcoplasmic reticulum micro-architecture and altered t-tubule structure in human heart failure. *J Muscle Res Cell Motil* 2006;**27**:297–306.
12. Louch WE, Mørk HK, Sexton J, Strømme TA, Laake P, Sjaastad I, Sejersted OM. T-tubule disorganization and reduced synchrony of Ca2+ release in murine cardiomyocytes following myocardial infarction. *J Physiol (Lond)* 2006;**574**:519–533.
13. Song L-S, Sobie EA, McCulle S, Lederer WJ, Balke CW, Cheng H. Orphaned ryanodine receptors in the failing heart. *Proc Natl Acad Sci U S A* 2006;**103**:4305–4310.
14. Ferrantini C, Crocini C, Coppini R, Vanzi F, Tesi C, Cerbai E, Poggesi C, Pavone FS, Sacconi L. The transverse-axial tubular system of cardiomyocytes. *Cell Mol Life Sci* 2013;**70**:4695–4710.
15. Heinzel FR, Bito V, Biesmans L, Wu M, Detre E, von Wegner F, Claus P, Dymarkowski S, Maes F, Bogaert J, Rademakers F, D'hooge J, Sipido K. Remodeling of T-tubules and reduced synchrony of Ca2+ release in myocytes from chronically ischemic myocardium. *Circ Res* 2008;**102**:338–346.
16. Litwin SE, Zhang D, Bridge JH. Dyssynchronous Ca(2+) sparks in myocytes from infarcted hearts. *Circ Res* 2000;**87**:1040–1047.
17. Louch WE, Bito V, Heinzel FR, Macianskiene R, Vanhaecke J, Flameng W, Mubagwa K, Sipido KR. Reduced synchrony of Ca2+ release with loss of T-tubules-a comparison to Ca2+ release in human failing cardiomyocytes. *Cardiovasc Res* 2004;**62**:63–73.
18. Dries E, Santiago DJ, Johnson DM, Gilbert G, Holemans P, Korte SM, Roderick HL, Sipido KR. Calcium/calmodulin-dependent kinase II and nitric oxide synthase 1-dependent modulation of ryanodine receptors during β-adrenergic stimulation is restricted to the dyadic cleft. *J Physiol* 2016;**594**:5923–5939.
19. Dries E, Bito V, Lenaerts I, Antoons G, Sipido KR, Macquaide N. Selective modulation of coupled ryanodine receptors during microdomain activation of calcium/calmodulin-dependent kinase II in the dyadic cleft. *Circ Res* 2013;**113**:1242–1252.
20. Fischer TH, Herting J, Tirilomis T, Renner A, Neef S, Toischer K, Ellenberger D, Förster A, Schmitto JD, Gummert J, Schöndube FA, Hasenfuss G, Maier LS, Sossalla S. Ca2+/calmodulin-dependent protein kinase II and protein kinase A differentially regulate sarcoplasmic reticulum Ca2+ leak in human cardiac pathology. *Circulation* 2013;**128**:970–981.
21. Walweel K, Molenaar P, Imtiaz MS, Denniss A, Dos Remedios C, Helden DF. V, Dulhunty AF, Laver DR, Beard NA. Ryanodine receptor modification and regulation by intracellular Ca2+ and Mg2+ in healthy and failing human hearts. *J Mol Cell Cardiol* 2017;**104**:53–62.
22. Biesmans L, Macquaide N, Heinzel FR, Bito V, Smith GL, Sipido KR. Subcellular heterogeneity of ryanodine receptor properties in ventricular myocytes with low T-tubule density. *PloS One* 2011;**6**:e25100.
23. Belevych AE, Ho H-T, Bonilla IM, Terentyeva R, Schober KE, Terentyev D, Carnes CA, Györke S. The role of spatial organization of Ca(2+) release sites in the generation of arrhythmogenic diastolic Ca(2+) release in myocytes from failing hearts. *Basic Res Cardiol* 2017;**112**:44.
24. Hilliard FA, Steele DS, Laver D, Yang Z, Le Marchand SJ, Chopra N, Piston DW, Huke S, Knollmann BC. Flecainide inhibits arrhythmogenic Ca2+ waves by open state block of ryanodine receptor Ca2+ release channels and reduction of Ca2+ spark mass. *J Mol Cell Cardiol* 2010;**48**:293–301.
25. Liu N, Ruan Y, Denegri M, Bachetti T, Li Y, Colombi B, Napolitano C, Coetzee WA, Priori SG. Calmodulin kinase II inhibition prevents arrhythmias in RyR2(R4496C+/-) mice with catecholaminergic polymorphic ventricular tachycardia. *J Mol Cell Cardiol* 2011;**50**:214–222.
26. Shan J, Xie W, Betzenhauser M, Reiken S, Chen B-X, Wronska A, Marks AR. Calcium leak through ryanodine receptors leads to atrial fibrillation in 3 mouse models of catecholaminergic polymorphic ventricular tachycardia. *Circ Res* 2012;**111**:708–717.
27. Galan DT, Bito V, Claus P, Holemans P, Abi-Char J, Nagaraju CK, Dries E, Vermeulen K, Ventura-Clapier R, Sipido KR, Driesen RB. Reduced mitochondrial respiration in the ischemic as well as in the remote non-ischemic region in post-myocardial infarction remodeling. *Am J Physiol Heart Circ Physiol* 2016;**311**:H1075–H1090.
28. Sipido KR, Stankovicova T, Flameng W, Vanhaecke J, Verdonck F. Frequency dependence of Ca2+ release from the sarcoplasmic reticulum in human ventricular myocytes from end-stage heart failure. *Cardiovasc Res* 1998;**37**:478–488.
29. Prosser BL, Ward CW, Lederer WJ. X-ROS signaling: rapid mechano-chemo transduction in heart. *Science* 2011;**333**:1440–1445.
30. Hare JM, Stamler JS. NO/redox disequilibrium in the failing heart and cardiovascular system. *J Clin Invest* 2005;**115**:509–517.
31. Damy T, Ratajczak P, Shah AM, Camors E, Marty I, Hasenfuss G, Marotte F, Samuel J-L, Heymes C. Increased neuronal nitric oxide synthase-derived NO production in the failing human heart. *Lancet Lond Engl* 2004;**363**:1365–1367.
32. Kostin S, Scholz D, Shimada T, Maeno Y, Mollnau H, Hein S, Schaper J. The internal and external protein scaffold of the T-tubular system in cardiomyocytes. *Cell Tissue Res* 1998;**294**:449–460.
33. Lyon AR, MacLeod KT, Zhang Y, Garcia E, Kanda GK, Lab MJ, Korchev YE, Harding SE, Gorelik J. Loss of T-tubules and other changes to surface topography in

ventricular myocytes from failing human and rat heart. *Proc Natl Acad Sci U S A* 2009; **106**:6854–6859.

34. Crossman DJ, Young AA, Ruygrok PN, Nason GP, Baddelely D, Soeller C, Cannell MB. T-tubule disease: relationship between t-tubule organization and regional contractile performance in human dilated cardiomyopathy. *J Mol Cell Cardiol* 2015;**84**: 170–178.

35. Seidel T, Navankasattusas S, Ahmad AA, Diakos NA, Xu WD, Tristani-Firouzi M, Bonios M, Taleb I, Li DY, Selzman CH, Drakos SG, Sachse FB. Sheet-like remodeling of the transverse tubular system in human heart failure impairs excitation-contraction coupling and functional recovery by mechanical unloading. *Circulation* 2017;**135**:1632–1645.

36. Sachse FB, Torres NS, Savio-Galimberti E, Aiba T, Kass DA, Tomaselli GF, Bridge JH. Subcellular structures and function of myocytes impaired during heart failure are restored by cardiac resynchronization therapy. *Circ Res* 2012;**110**:588–597.

37. Sossalla S, Fluschnik N, Schotola H, Ort KR, Neef S, Schulte T, Wittköpper K, Renner A, Schmitto JD, Gummert J, El-Armouche A, Hasenfuss G, Maier LS. Inhibition of elevated Ca2+/calmodulin-dependent protein kinase II improves contractility in human failing myocardium. *Circ Res* 2010;**107**:1150–1161.

38. Piacentino V, Weber CR, Chen X, Weisser-Thomas J, Margulies KB, Bers DM, Houser SR. Cellular basis of abnormal calcium transients of failing human ventricular myocytes. *Circ Res* 2003;**92**:651–658.

39. Acsai K, Antoons G, Livshitz L, Rudy Y, Sipido KR. Microdomain [Ca^{2+}] near ryanodine receptors as reported by L-type Ca^{2+} and Na+/Ca^{2+} exchange currents. *J Physiol* 2011;**589**:2569–2583.

40. Glukhov AV, Balycheva M, Sanchez-Alonso JL, Ilkan Z, Alvarez-Laviada A, Bhogal N, Diakonov I, Schobesberger S, Sikkel MB, Bhargava A, Faggian G, Punjabi PP, Houser SR, Gorelik J. Direct evidence for microdomain-specific localization and remodeling of functional l-type calcium channels in rat and human atrial myocytes. *Circulation* 2015;**132**:2372–2384.

41. Bryant SM, Kong CHT, Watson J, Cannell MB, James AF, Orchard CH. Altered distribution of ICa impairs Ca release at the t-tubules of ventricular myocytes from failing hearts. *J Mol Cell Cardiol* 2015;**86**:23–31.

42. Sobie EA, Guatimosim S, Gómez-Viquez L, Song L-S, Hartmann H, Saleet Jafri M, Lederer WJ. The Ca 2+ leak paradox and rogue ryanodine receptors: sR Ca 2+ efflux theory and practice. *Prog Biophys Mol Biol* 2006;**90**:172–185.

43. Baddeley D, Jayasinghe ID, Lam L, Rossberger S, Cannell MB, Soeller C. Optical single-channel resolution imaging of the ryanodine receptor distribution in rat cardiac myocytes. *Proc Natl Acad Sci U S A* 2009;**106**:22275–22280.

44. Macquaide N, Tuan H-TM, Hotta J-I, Sempels W, Lenaerts I, Holemans P, Hofkens J, Jafri MS, Willems R, Sipido KR. Ryanodine receptor cluster fragmentation and redistribution in persistent atrial fibrillation enhance calcium release. *Cardiovasc Res* 2015; **108**:387–398.

45. Erickson JR, Nichols CB, Uchinoumi H, Stein ML, Bossuyt J, Bers DM. S-nitrosylation induces both autonomous activation and inhibition of calcium/calmodulin-dependent protein kinase II δ. *J Biol Chem* 2015;**290**:25646–25656.

46. Dhar-Chowdhury P, Harrell MD, Han SY, Jankowska D, Parachuru L, Morrissey A, Srivastava S, Liu W, Malester B, Yoshida H, Coetzee WA. The glycolytic enzymes, glyceraldehyde-3-phosphate dehydrogenase, triose-phosphate isomerase, and pyruvate kinase are components of the K(ATP) channel macromolecular complex and regulate its function. *J Biol Chem* 2005;**280**:38464–38470.

47. Neglia D, De Caterina A, Marraccini P, Natali A, Ciardetti M, Vecoli C, Gastaldelli A, Ciociaro D, Pellegrini P, Testa R, Menichetti L, L'Abbate A, Stanley WC, Recchia FA. Impaired myocardial metabolic reserve and substrate selection flexibility during stress in patients with idiopathic dilated cardiomyopathy. *Am J Physiol Heart Circ Physiol* 2007;**293**:H3270–H3278.

48. Purohit A, Rokita AG, Guan X, Chen B, Koval OM, Voigt N, Neef S, Sowa T, Gao Z, Luczak ED, Stefansdottir H, Behunin AC, Li N, El-Accaoui RN, Yang B, Swaminathan PD, Weiss RM, Wehrens XHT, Song L-S, Dobrev D, Maier LS, Anderson ME. Oxidized Ca(2+)/calmodulin-dependent protein kinase II triggers atrial fibrillation. *Circulation* 2013;**128**:1748–1757.

49. Respress JL, Oort RJ. V, Li N, Rolim N, Dixit SS, deAlmeida A, Voigt N, Lawrence WS, Skapura DG, Skårdal K, Wisløff U, Wieland T, Ai X, Pogwizd SM, Dobrev D, Wehrens XHT. Role of RyR2 phosphorylation at S2814 during heart failure progression. *Circ Res* 2012;**110**:1474–1483.

50. Luo M, Guan X, Luczak ED, Lang D, Kutschke W, Gao Z, Yang J, Glynn P, Sossalla S, Swaminathan PD, Weiss RM, Yang B, Rokita AG, Maier LS, Efimov IR, Hund TJ, Anderson ME. Diabetes increases mortality after myocardial infarction by oxidizing CaMKII. *J Clin Invest* 2013;**123**:1262–1274.

51. Wojciechowska C, Romuk E, Tomasik A, Skrzep-Poloczek B, Nowalany-Kozielska E, Birkner E, Jacheć W. Oxidative stress markers and C-reactive protein are related to severity of heart failure in patients with dilated cardiomyopathy. *Mediators Inflamm* 2014;**2014**:1.

52. Dai D-F, Johnson SC, Villarin JJ, Chin MT, Nieves-Cintrón M, Chen T, Marcinek DJ, Dorn GW, Kang YJ, Prolla TA, Santana LF, Rabinovitch PS. Mitochondrial oxidative stress mediates angiotensin II-induced cardiac hypertrophy and Galphaq overexpression-induced heart failure. *Circ Res* 2011;**108**:837–846.

53. Gauthier LD, Greenstein JL, O'rourke B, Winslow RL. An integrated mitochondrial ROS production and scavenging model: implications for heart failure. *Biophys J* 2013; **105**:2832–2842.

54. Kohlhaas M, Liu T, Knopp A, Zeller T, Ong MF, Bohm M, O'Rourke B, Maack C. Elevated cytosolic Na+ increases mitochondrial formation of reactive oxygen species in failing cardiac myocytes. *Circulation* 2010;**121**:1606–1613.

55. Curran J, Hinton MJ, Ríos E, Bers DM, Shannon TR. Beta-adrenergic enhancement of sarcoplasmic reticulum calcium leak in cardiac myocytes is mediated by calcium/calmodulin-dependent protein kinase. *Circ Res* 2007;**100**:391–398.

56. Liu N, Napolitano C, Venetucci LA, Priori SG. Flecainide and antiarrhythmic effects in a mouse model of catecholaminergic polymorphic ventricular tachycardia. *Trends Cardiovasc Med* 2012;**22**:35–39.

57. Swaminathan PD, Purohit A, Hund TJ, Anderson ME. Calmodulin-dependent protein kinase II: linking heart failure and arrhythmias. *Circ Res* 2012;**110**:1661–1677.

58. Wagner S, Rokita AG, Anderson ME, Maier LS. Redox regulation of sodium and calcium handling. *Antioxid Redox Signal* 2013;**18**:1063–1077.

59. Xie L-H, Chen F, Karagueuzian HS, Weiss JN. Oxidative-stress-induced afterdepolarizations and calmodulin kinase II signaling. *Circ Res* 2009;**104**:79–86.

60. Bovo E, Martin JL, Tyryfter J, Tombe PP. D, Zima AV. R-CEPIA1er as a new tool to directly measure sarcoplasmic reticulum [Ca] in ventricular myocytes. *Am J Physiol Heart Circ Physiol* 2016;**311**:H268–H275.

61. Despa S, Shui B, Bossuyt J, Lang D, Kotlikoff MI, Bers DM. Junctional cleft [Ca^{2+}]i measurements using novel cleft-targeted Ca^{2+} sensors. *Circ Res* 2014;**115**:339–347.

62. Shang W, Lu F, Sun T, Xu J, Li L-L, Wang Y, Wang G, Chen L, Wang X, Cannell MB, Wang S-Q, Cheng H. Imaging Ca2+ nanosparks in heart with a new targeted biosensor. *Circ Res* 2014;**114**:412–420.

63. Li H, Lichter JG, Seidel T, Tomaselli GF, Bridge JHB, Sachse FB. Cardiac resynchronization therapy reduces subcellular heterogeneity of ryanodine receptors, T-tubules, and Ca2+ sparks produced by dyssynchronous heart failure. *Circ Heart Fail* 2015;**8**: 1105–1114.